VII International Conference on Particle-Based Methods
PARTICLES 2021
P. Wriggers, M. Bischoff, E. Oñate, M. Bischoff, A. Düster & T. Zohdi (Eds)

IMPROVING THE PREDICTION ABILITY OF SIMPLIFIED DISCRETE ELEMENT MODELS ON COMPLEX LOADING PATHS

Bilal Al Tfaily[1,2,*], Luc Sibille[1], Rodaina Aboul Hosn[2] and Abdelkrim Bennabi[2]

[1] Univ. Grenoble Alpes, CNRS, Grenoble INP, 3SR
1270 Rue de la Piscine, F-38000 Grenoble, France
Email: bilal.al-tfaily@3sr-grenoble.fr - luc.sibille@3sr-grenoble.fr

[2] Institut de Recherche en Constructibilité (IRC)
École Spéciale des Travaux Publics, du bâtiment et de l'industrie (ESTP)
28 avenue du Président Wilson, 94234 Paris, France
Email: raboulhosn@estp-paris.eu - abennabi@estp-paris.eu

Key words: DEM, Soil Constitutive Behavior, Triaxial Loading Paths

Abstract. Discrete element method has been proved to be an effective method in predicting quantitatively the constitutive response of soils, even in the case of complex loadings (with rotation of principal stress directions, or loading/unloading cycles) where conventional elasto-plastic constitutive relations may fail to simulate realistic responses [10]. For granular soils with a narrow grading, a direct representation of soil grains by polyhedral particles or with the level set method is possible [5], whereas for finer soils, or soils with a wider grading, alternative solutions should be considered. Spherical particles with enriched contact laws (e.g. by introducing rolling resistance at the contact) or rather simplified clumps of spheres can be used. This study aims to compare such different approaches. This comparison is done in terms of the prediction abilities at the macroscopic scale of the constitutive responses of soils, in particular for complex loading paths. Two kinds of discrete models are considered: (i) spherical particles with a rolling resistance, (ii) simple clumps made of 2 to 6 spheres. The models are calibrated from two drained triaxial compressions on dense and loose Hostun sand samples. They are then assessed, according to the macroscopic response, on loading paths strongly different from the calibration loading paths (isochoric compressions, circular stress paths in the deviatoric strain plane, constant deviatoric stress path, ...). The objective is to produce an optimized discrete element model in terms of prediction ability with respect to the computational cost, able to represent natural soils with possibly a wide particle size distribution, in order to tackle boundary value problems (as geotechnical structures) subjected to complex loadings.

1 INTRODUCTION

The discrete element method (DEM) [3] has been widely used to predict the constitutive behavior of soils. To prevent the complexity of the models and decrease the computational cost due to contact detection and forces calculations, spheres have been used [1, 9, 10] to represent the grains. However, it has been shown that these models (calibrated on triaxial compression tests) need improvement to predict the mechanical response in case of some complex loadings

even when the contact law is enriched by adding non-constant friction angle and initial connectivity control [9], or using different simple shape such as a clump of two spheres [10]. The particle shape (angularity – anisotropy – roughness) plays an important role in the constitutive behavior of soils. Recent studies [5] offer the possibility to reproduce the real grain shape. However, such approach does not work in case of non-granular soils or fine soils such as clay and silt, and is very expensive in computational cost. Therefore, the goal of this work is to check on one hand if more complex particle shapes than spheres (clumps) are able to improve the predictions of the models and, on the other hand to check the trade-off between the rolling resistance and the use of clumps in terms of prediction ability. It is important to keep in mind that the computational cost should be limited so that the chosen model can be used to tackle boundary value problems for application in geotechnical engineering.

In the first part of this paper the different models and sample preparation methods are defined. After that we present the calibration of the model based on triaxial compression tests on dense and loose Hostun sand. Then the models are validated on the complex loading paths. Finally, we discuss in the conclusion the main findings of this work.

2 DISCRETE NUMERICAL MODELS

2.1 Particle shapes and contact laws

Three 3D discrete element models have been created using YADE software to simulate the mechanical behavior of a granular material. The models differ from the shape of the particles as represented in Figure 1.

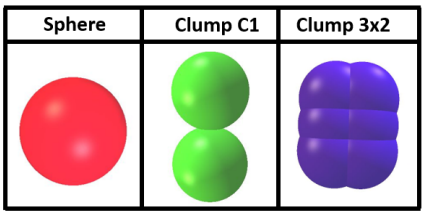

Figure 1: Particles shapes (from left to right): sphere - clump of two spheres - clump of six spheres

For the 1^{st} model, particles are made of a single elementary sphere, whereas particles for the two other models are constituted by a clump. The clump C1 made of two juxtaposed spheres is used for the 2^{nd} model, and clump 3x2 made with an aggregate of 6 spheres is used for the 3^{rd} model. In the following the name of the particles (sphere, C1 and 3x2) is used to name the three models.

All models in this paper are built considering a classical Colombian friction inter-granular contact law. For a couple of particles with radii R_1 and R_2 in contact with an overlap δ_n and normal $\vec{n}$, the normal and shear forces are given respectively by:

$$\vec{F_n} = k_n \, \delta_n \, \vec{n} \tag{1}$$

$$\Delta\vec{F_s} = -k_s \, \Delta\vec{u}_s \;\; with \;\; ||\vec{F_s}|| \leq \mu \, ||\vec{F_n}|| \tag{2}$$

Where k_n and k_s are the normal and tangential stiffnesses considered constant, and φ_c the contact friction angle. The shear force $\vec{F}_s$ is computed incrementally from the relative shear displacement at contact point $\vec{u}_s$.

To prevent excessive rotations that cause unrealistic shear strengths in the sphere and C1 models, the contact law is completed by a rolling moment acting against the relative rotation $\vec{\theta}_r$ of the particles. Rolling moment $\vec{M}_r$ is defined by the rolling stiffness, k_r, and a threshold represented by the rolling friction coefficient η_r:

$$\Delta\overrightarrow{M_r} = -k_r\Delta\overrightarrow{\theta_r} \;\; with \;\; || \overrightarrow{M_r} ||\leq|| \overrightarrow{F_n} || \, \eta_r \, min(R_1, R_2) \tag{3}$$

For the model 3x2, no inter-granular rolling moment is added, since the shape of the six clustered spheres is sufficiently non spherical to overcome the issue of unrealistic shear strength as it is shown in the calibration section further in the paper. Dependency of the macroscopic elastic properties on the particle sized is avoided by defining the contact stiffnesses from the stiffness modulus E_c, and the dimensionless shear α_s and rolling α_r stiffness coefficients as follows:

$$k_n = 2E_c\frac{R1R2}{R1+R2} \; ; \; k_s = \alpha_s k_n \; ; \; k_r = \alpha_r R1R2k_s \tag{4}$$

3 CALIBRATION OF THE MODELS

3.1 Controlling the initial porosities of the models

An important parameter that controls the mechanical behavior of a granular material is its initial bulk porosity n_0. In particular, the difference between the initial porosity of the soil and the one at the critical state reflects its ability to produce dilation and higher shear strength. Consequently, in the discrete models it is essential to choose the right way to define values of initial porosities to produce the same volumetric change as the experiment. Three different options can be followed to choose the initial porosity. First and second options consist to assign the same initial porosity or same relative density, respectively, of the numerical granular assembly as the ones of the real soil sample. However, if the shapes of the grains of the numerical model are different than the real ones, it is not insured that the model will produce the same volumetric deformation. Thus, we use the third option in this work where we define the initial absolute numerical porosity that results in the same volumetric deformation as the real soil. In other words, the initial porosity is chosen such that the ratio r defined in Eq. 5 is identical experimentally and numerically. r depends on the state parameter ψ (Eq. 6) which is the difference between the void ratios at the initial, e_i, and critical, e_c, states respectively:

$$r = \frac{\psi}{(1+e_i)} = \frac{\Delta V}{V_i} \tag{5}$$

$$\psi = e_i - e_c = \frac{V_{vi}}{V_s} - \frac{V_{vc}}{V_s} = \frac{\Delta V}{V_i}(1+e_i) \tag{6}$$

Where V_{vi} and V_{vc} are the volume of voids at the initial and critical states respectively, and Vs is the volume of solids. Hence, the initial porosity to assign to the numerical assembly can

be deduced from the void ratios at the critical state for the numerical and experimental samples and the initial void ratio of the experimental sample.

In the case of some very loose soils, it is impossible to reach the required initial porosity of the numerical granular assembly without the addition of adhesion during the initial sample compaction as it was proposed in [1], similarly to the experimental reconstitution technique of soil samples by the moist tamping method.

3.2 Calibration methodology

In this section the calibration methodology is defined to calibrate the different parameters of the model from drained triaxial compressions performed on Hostun sand. Following [1], elastic parameters such as the contact stiffness E_c or the rolling stiffness coefficient α_r are chosen high enough so that they do not affect the plastic macroscopic properties.

Then, the calibration methodology is divided into two main steps. The first step consists in fitting the shear strength at the critical state. The latter depends on the rolling friction (if used), the shape of the particles and the contact friction angle. Nevertheless, the influence of the contact friction angle on the critical shear strength is negligible if it is greater than 15 degree [1]. Therefore, in this step the rolling friction of the sphere and clump C1 models respectively is calibrated. Concerning the 3x2 model, we calibrate the distance D between the spheres of clump 3x2 (D=0.7xR) to reach the required shear strength at the critical state (Figure. 2).

Besides, peak shear strength, for an initial dense granular assembly, and the volumetric deformation depend on the rolling friction (if any), the particle shape, the contact friction angle and the initial porosity. Nevertheless, the rolling friction (for sphere and C1 models) and the particle shape (for 3x2 model) were already calibrated in the first step. Consequently, in a second step the initial porosity is chosen such that the ratio r (Eq. 5) is the same numerically and experimentally and the contact friction angle is calibrated in order to fit the peak shear strength.

3.3 Calibrated models

A parallelepipedic periodic cell made up of 10000 particles have been considered in each of the models. The calibration methodology has been applied to calibrate the parameters from two experimental drained triaxial compression on dense (confining pressure p_c = 350 KPa) and loose (confining pressure p_c = 300 KPa) Hostun sand RF. For the three models, the particle size distribution of the numerical assemblies is almost identical to that of the Hostun sand. The identified parameters of the models are given in (Table 1) and simulated calibration paths are presented in Figure 3. By calibrating the ratio r, we are able to obtain numerical relative volumetric changes close to the experimental ones. Furthermore, it is important to highlight that experimental and numerical sample porosities are different (initially and at the critical state; see Figure 3c) because the numerical granular assemblies are not exact reproductions of the sand samples but voluntarily simplified descriptions. Finally, porosities of the experimental loose and dense sand samples at the critical state are different because experimentally the global porosity is calculated with no consideration of the shear band in dense samples [11], contrary to the numerical simulations where porosities at the critical state are identical for initially loose and dense samples as no meaningful strain localization occurs.

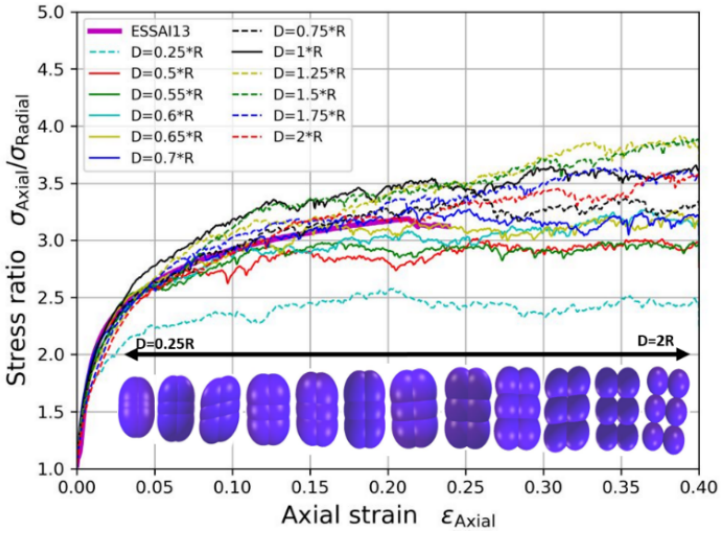

Figure 2: Calibration of the shear strength at the critical state of clump 3x2 model with respect to a drained triaxial compression on a loose Hostun sand. D represents the distance between the centres of the spheres of radius R composing the 3x2 clumps.

Table 1: Parameters of the discrete numerical models identified from the calibration on dense and loose Hostun sand RF. D represents the distance between the centres of the spheres of radius R composing the 3x2 clumps (see Figure 2).

	n_0 *loose*	n_0 *dense*	$E_C(MPa)$	α_s	α_r	$\varphi_c(^\circ)$	η_r	D
Sphere	0.419	0.357	500	0.5	3	21	0.25	-
C1	0.467	0.407	500	0.5	3	37.5	0.07	-
3x2	0.387	0.322	500	0.5	3	37	-	0.7xR

4 VALIDATION OF THE MODELS

4.1 Model validation on dense sand

4.1.1 Cyclic compression/extension loading path

This path is performed by applying a cyclic axisymmetric ($\sigma_2 = \sigma_3$) compression/extension loading at constant mean pressure. The mean pressure is fixed at 200 kPa and cycles are performed by controlling the axial strain ε_1 such that $\Delta\varepsilon_1 = 3.8\%$ for each cycle, except the first one with a bigger amplitude. Hence, σ_1 constitutes a response parameter.

The numerical response is compared to the experimental test carried out by [12] (Figure 4). The numerical response, using the calibrated parameters found in the previous section, is close to the experimental one for the different particle's shape considered. However, the sphere model presents a better quantitative prediction in particular with a faithful description of the volumetric deformation and a good estimation of the overall stiffness along cycles. It is important

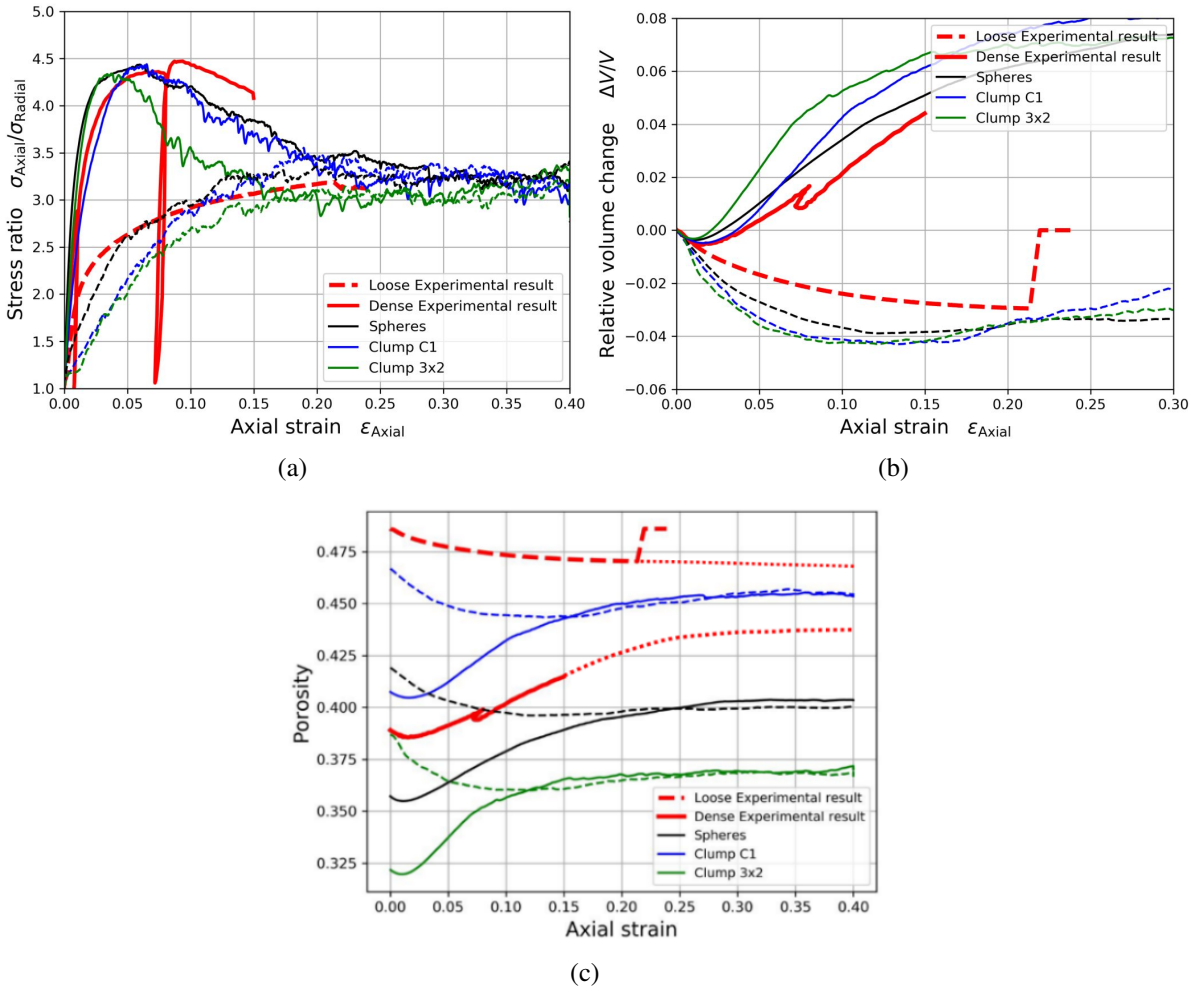

Figure 3: Calibration of the discrete element models made of particles with different shapes and based on drained triaxial compressions on dense and loose Hostun sand.

to note that conventional elasto-plastic constitutive relations would require additional history parameters (usually calibrated on cyclic tests) in order to model the soil response to such tests.

4.1.2 Circular stress loading path

The models are also validated on a circular loading stress path in the deviatoric stress plane, by continuously changing the Lode angle φ_σ and keeping the mean pressure and the deviatoric stress constant [8]. The Lode angle is defined with respect to the axis s_1 which is the projection of the σ_1 axis on the deviatoric plane. The stress deviator intensity is defined by the second stress invariant:

$$I_{2\sigma} = \sqrt{\mathrm{tr}\left(\mathbf{s}^2\right)} \tag{7}$$

Where **s** is the deviatoric stress tensor. Initially, the soil sample is compressed isotropically to p_c = 500 KPa, subsequently a compression in direction 3 (i.e. $\varphi_\sigma = -120^o$) with a constant mean

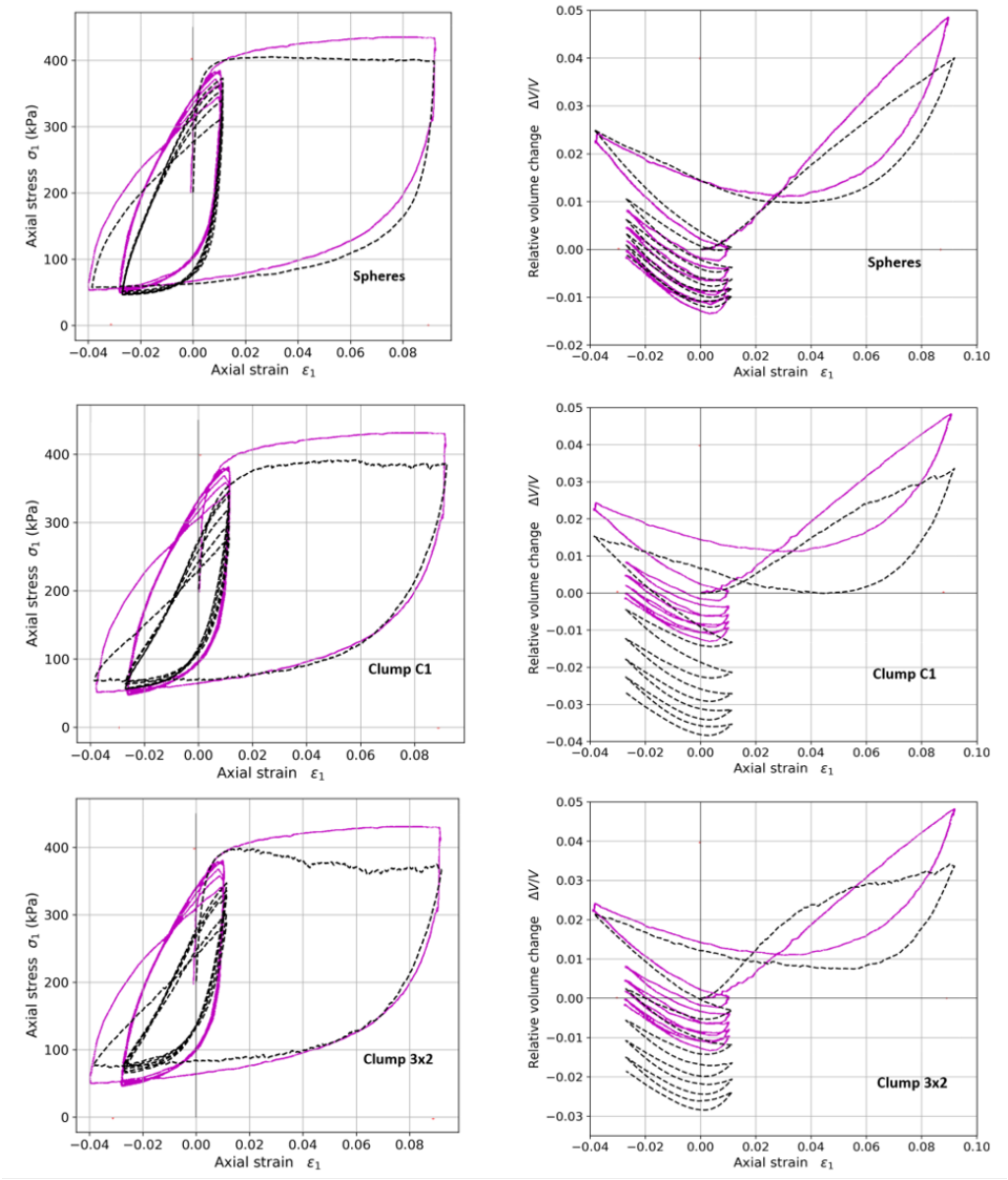

Figure 4: Validation on cyclic compression/extension paths with constant mean pressure on dense Hostun sand: experimental results are plotted with the continuous magenta lines and simulated responses are represented with the dashed black lines.

pressure p=p_c, to reach a value of $I_{2\sigma}$ = 420 KPa. Eventually the circular path is executed. It is constituted of two revolutions in the deviatoric stress plane by changing φ_σ between -120^o and $+600^o$.

The numerical models response is compared to the experimental one obtained by Lanier and Zitouni [6] in Figure 5. All models underestimate the contractancy observed experimentally, however the sphere and C1 models give a global trend of the volumetric deformations in agreement with the experimental data. The 3x2 model diverges from the experimental data by

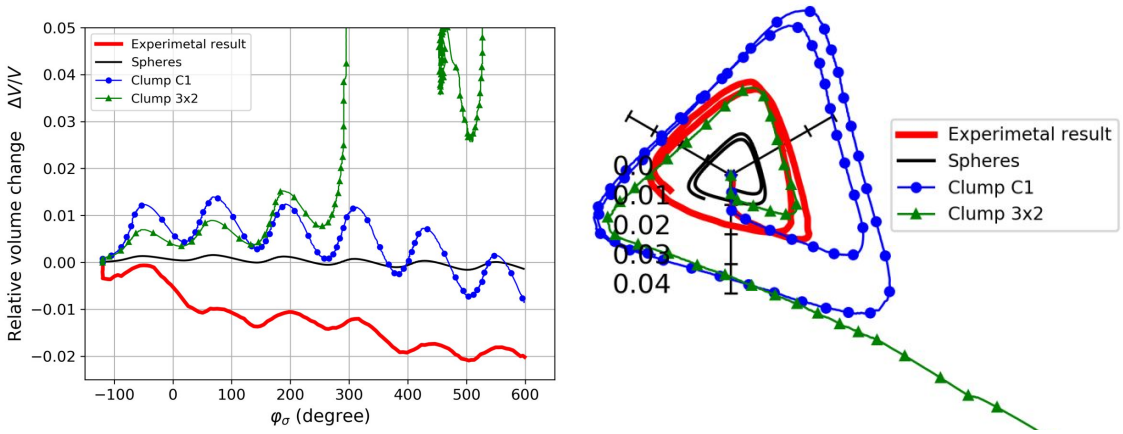

(a) (b)

Figure 5: Validation from a circular stress loading path on dense Hostun sand: the relative volume change is represented in terms of the Lode angle (left), the strain response path is projected on the deviatoric strain plane (right).

describing a strong dilation of the numerical sample leading to its failure. Finally, the sphere model underestimates the deviatoric deformations, whereas the C1 model overestimates them, but both models produce a response which is qualitatively realistic.

4.2 Model validation on loose sand

4.2.1 Isochoric compression

A conventional axisymmetric undrained compression (with p_c = 200 KPa) is considered from Benahmed [2]. Experimentally, the saturated and compressed sand undergoes isochoric deformation. Numerically, the isochoric condition is directly imposed by controlling the radial strains so that it is equal to the axial strain (i.e., $\varepsilon_{\text{radial}} = \varepsilon_{\text{axial}}/2$). The experimental results and simulated responses are shown in Figure 6.

It shows that the three models fail to predict the experimental response, where a complete liquefaction is observed at low axial strain numerically, without reaching the q-peak. Experimentally the liquefaction requires a larger deformation of the samples. The angular or anistropic shaped particles of the real sand may explain the different response experimentally. In addition, the use of the rolling friction parameter with spheres and clump C1 or the more complex shape 3x2 may not be enough to describe the particles interlocking under the global isochoric constraint.

4.2.2 q-constant path

The constant stress deviator loading path consists of keeping the stress deviator q constant and decreasing the mean pressure p after reaching a stress state from a preliminary drained compression. We consider an experimental test performed by Daouadji et al. [4], with an initial

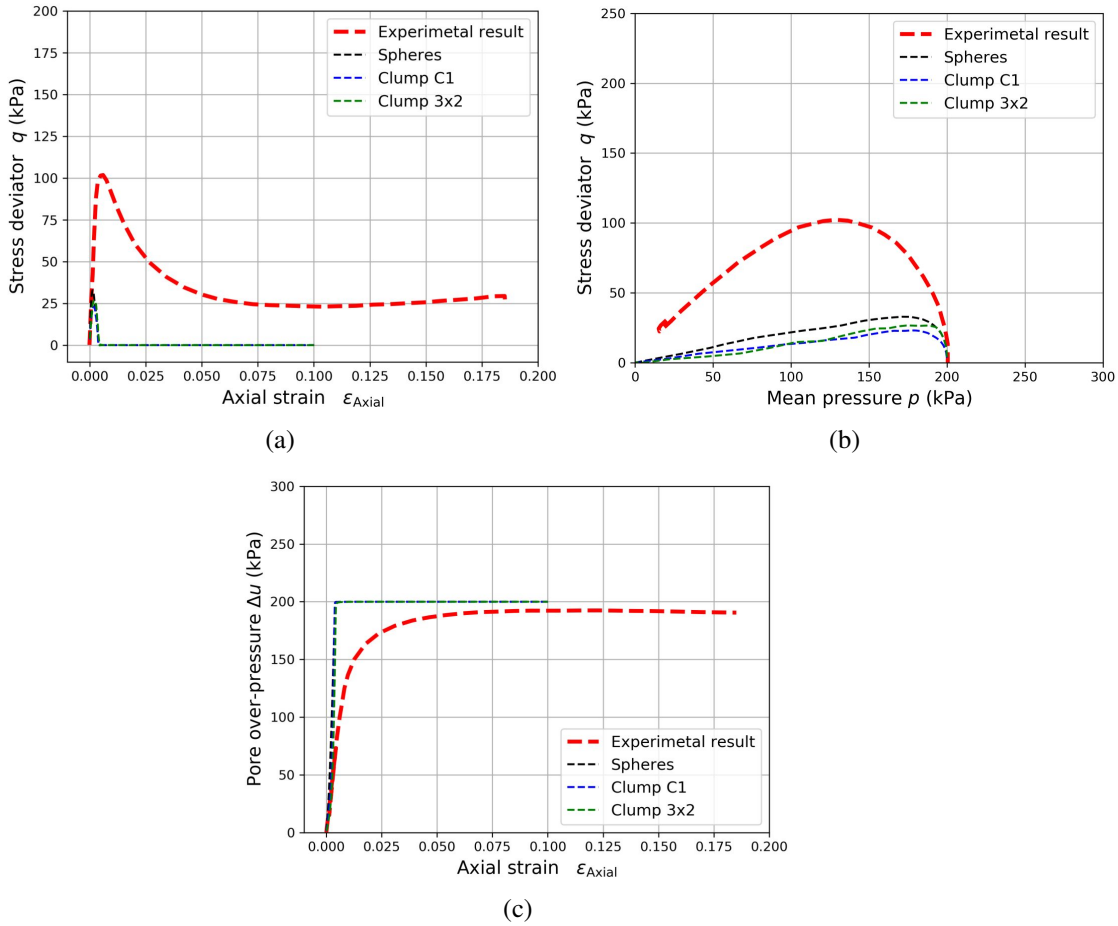

Figure 6: Validation on undrained axisymmetric compressions on loose Hostun sand, comparison with experimental test with p_c = 200 kPa .

confinement p_c = 300 kPa and a stress deviator q = 119 kPa reached after the initial drained compression.

The comparison between the numerical and experimental responses is shown in Figure 7. The models reproduce correctly the initial drained compression. However, they behave opposite to the sand response along the q-constant path. The models present a contraction of the granular assemblies whereas a dilation is observed experimentally. However the failure stress state in the q-p plane is rather well predited by the models (Figure 7c).

5 CONCLUSION

In this paper we investigated two options to overcome the much simple shape of spheres: rolling friction or non-spherical shape (but still simple) with a 3rd option consisting in mixing the two options. The quality of the simulated responses for the calibration is close for all the models, even if the description brought by the sphere model is slightly better. In terms of computational cost, the model with spheres is the least consuming while the 3x2 model is the most one. However, the complexity of the calibration process is similar for all the models.

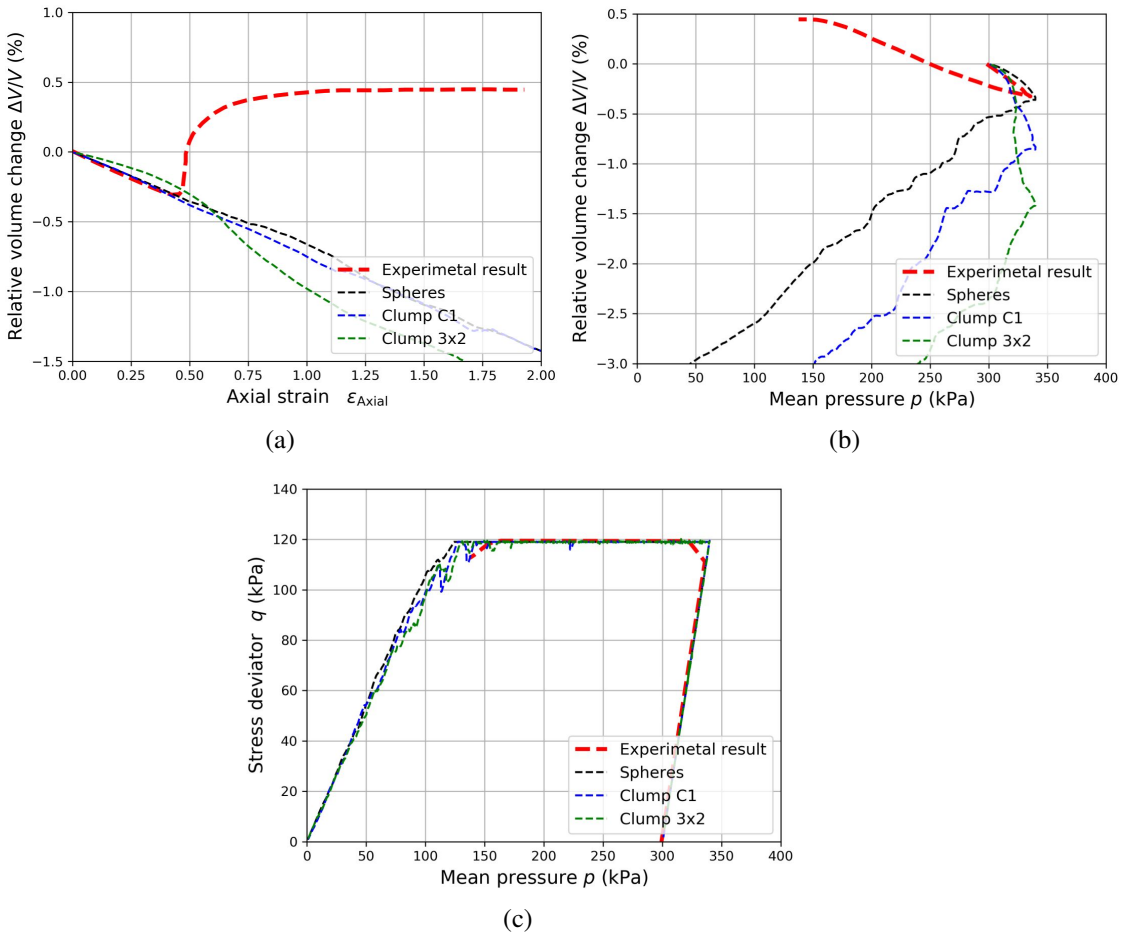

Figure 7: Validation on constant stress deviator loading paths on loose Hostun sand, comparison with experimental test with q = 119 kPa.

The models were validated with respect to two initial density states. On one hand, the validation from a dense initial state shows that, even if the prediction with the sphere model is not fully in agreement with the experimental data (in particular for the circular stress loading path), it gives a better prediction than the other models. On the other hand, the validation on loose initial states shows that all the models fail. This may not be due to the loose initial state but could be related to the impact of the important decrease of the mean pressure along the considered loading paths on the constitutive soil response which is not correctly taken into account in the definition of the models.

Despite the limitation of the models, the model of spheres with rolling resistance is the one representing the lower computation cost together with the best prediction ability (among the three models tested) and represents a good compromise. Finally, to improve the prediction ability of the models in particular along loading paths with important changes of mean pressure, we may use angular shaped particles or take into account the roughness of the particles [7]. The latter could be implemented by introducing a contact friction angle as a function of the normal contact stress.

REFERENCES

[1] Aboul Hosn, R., Sibille, L., Benahmed, N., and Chareyre, B. Discrete numerical modeling of loose soil with spherical particles and interparticle rolling friction. *Granular matter 19*, 1 (2017), 1–12.

[2] Benhamed, N. Comportement mécanique d'un sable sous cisaillement monotone et cyclique: application aux phénomenes de liquéfaction et de mobilité cyclique. *These de doctorat de l'Ecole nationale des ponts et chaussées, France* (2001).

[3] Cundall, P. A., and Strack, O. D. A discrete numerical model for granular assemblies. *geotechnique 29*, 1 (1979), 47–65.

[4] Daouadji, A., Darve, F., Al Gali, H., Hicher, P., Laouafa, F., Lignon, S., et al. Diffuse failure in geomaterials: experiments, theory and modelling. *International Journal for Numerical and Analytical Methods in Geomechanics 35*, 16 (2011), 1731–1773.

[5] Kawamoto, R., Andò, E., Viggiani, G., and Andrade, J. E. All you need is shape: predicting shear banding in sand with ls-dem. *Journal of the Mechanics and Physics of Solids 111* (2018), 375–392.

[6] Lanier, J., and Zitouni, Z.-E.-A. Development of a data base using the grenoble true triaxial apparatus-constitutive equations for granular non cohesive soils. In *Proceedings of the international workshop on constitutive equations for granular non-cohesive soils, Balkema, Rotterdam, 22-24 July 1987* (1988).

[7] Mollon, G., Quacquarelli, A., Andò, E., and Viggiani, G. Can friction replace roughness in the numerical simulation of granular materials? *Granular Matter 22*, 2 (2020), 1–16.

[8] Saada, A. S., and Bianchini, G. Constitutive equations for granular non-cohesive soils. In *Proceedings of the international workshop on constitutive equations for granular non-cohesive soils, Balkema, Rotterdam, 22-24 July 1987, Cleveland* (1988), AA Balkema.

[9] Sibille, L., Benahmed, N., and Darve, F. Constitutive response predictions of both dense and loose soils with a discrete element model. *Computers and Geotechnics 135* (2021), 104161.

[10] Sibille, L., Villard, P., Darve, F., and Aboul Hosn, R. Quantitative prediction of discrete element models on complex loading paths. *International Journal for Numerical and Analytical Methods in Geomechanics 43*, 5 (2019), 858–887.

[11] Zhu, H., Nguyen, H. N., Nicot, F., and Darve, F. On a common critical state in localized and diffuse failure modes. *Journal of the Mechanics and Physics of Solids 95* (2016), 112–131.

[12] Zitouni, Z.-E.-A. *Comportement tridimensionnel des sables*. PhD thesis, Université Joseph Fourier (Grenoble), 1988.